

AD-A253 188

ATION PAGE

Form Approved
OMB No. 0704-0188



1a. REPORT SECURITY CLASSIFICATION
unclassified

1b. RESTRICTIVE MARKINGS

2

2a. SECURITY CLASSIFICATION
SECRET

2b. DECLASSIFICATION/DOWNGRADING SCHEDULE
1982

3. DISTRIBUTION/AVAILABILITY OF REPORT
approved for public release; distribution unlimited

4. PERFORMING ORGANIZATION REPORT NUMBER(S)

5. MONITORING ORGANIZATION REPORT NUMBER(S)
AFOSR F49620-88-C-0009

6a. NAME OF PERFORMING ORGANIZATION

6b. OFFICE SYMBOL
(if applicable)

7a. NAME OF MONITORING ORGANIZATION

Optical Sciences Center

ONRRR AFOSR-TR. 00 0688

6c. ADDRESS (City, State, and ZIP Code)

7b. ADDRESS (City, State, and ZIP Code)

University of Arizona
Tucson, Arizona 85721

University of New Mexico
Bandelier Hall West
Albuquerque, NM 87131

8a. NAME OF FUNDING/SPONSORING ORGANIZATION

8b. OFFICE SYMBOL
(if applicable)

9. PROCUREMENT INSTRUMENT IDENTIFICATION NUMBER

JSOP (AFOSR)

NE

AFOSR F49620-88-C-0009

8c. ADDRESS (City, State, and ZIP Code)

10. SOURCE OF FUNDING NUMBERS

Air Force Office of Scientific Research
Bolling Air Force Base, Washington DC 20332-6448

PROGRAM ELEMENT NO.	PROJECT NO.	TASK NO.	WORK UNIT ACCESSION NO.
61102	2301	A1	

11. TITLE (Include Security Classification)
Research in Optical Sciences

12. PERSONAL AUTHOR(S)
R.R. Shannon

13a. TYPE OF REPORT
final

13b. TIME COVERED
FROM 10/1/90 TO 9/30/91

14. DATE OF REPORT (Year, Month, Day)
1992 February 17

15. PAGE COUNT
53

16. SUPPLEMENTARY NOTATION

17. COSATI CODES		
FIELD	GROUP	SUB-GROUP

18. SUBJECT TERMS (Continue on reverse if necessary and identify by block number)
optical sciences

19. ABSTRACT (Continue on reverse if necessary and identify by block number)

This report covers special work carried out on the Joint Services Optics Program at the Optical Sciences Center during the period October 1, 1990 through September 30, 1991. The work summarized in the report, and detailed in the appendices, is responsive to request from two sponsors. In each case the work required system analysis and technical evaluation of the potential in two areas of optical technology: a high-speed video system; and work on membrane mirrors.

92-19945



20. DISTRIBUTION/AVAILABILITY OF ABSTRACT
 UNCLASSIFIED/UNLIMITED SAME AS RPT. DTIC USERS

21. ABSTRACT SECURITY CLASSIFICATION
unclassified

22a. NAME OF RESPONSIBLE INDIVIDUAL
Sandra L. Singer, S. Lassberg

22b. TELEPHONE (Include Area Code)
202-707-4906

22c. OFFICE SYMBOL
NE

Contract F49620-88-C-0009

RESEARCH IN THE OPTICAL SCIENCES

A Final Report Prepared for

**Air Force Office of Scientific Research
Joint Services Optics Program**

**Robert R. Shannon, Director
Optical Sciences Center
University of Arizona
Tucson, Arizona 85721**

Approved for public release, distribution unlimited.

For the period 1 October 1990 through 30 September 1991

INTRODUCTION

This report covers special work carried out at the University of Arizona, Optical Sciences Center under support provided through the Joint Services Optical Program (JSOP).

The work summarized in the report, and detailed in the appendices, is responsive to requests from two sponsors. In each case the work required system analysis and technical evaluation of the potential in two areas of optical technology. The work on a high-speed video system was led by Professor Eustace L. Dereniak. The work on membrane mirrors was led by Professor William L. Wolfe.

Robert R. Shannon
Director

Accession For	
NTIS GRA&I	<input checked="" type="checkbox"/>
DTIC TAB	<input type="checkbox"/>
Unannounced	<input type="checkbox"/>
Justification _____	
By _____	
Distribution/	
Availability Codes	
Dist	Avail and/or Special
A-1	

DTIC QUALITY INSPECTED 2

CONTENTS

Introduction	i
High-speed, High-resolution Video Imaging System	1
Vacuum Mirror Studies	7
Appendix A. Radiometric Calculations and Measurements	9
Appendix B. Expected Signal-to-Noise Ratio	25
Appendix C. Power Dissipation	29
Appendix D. Contrast Degradation Due to Integration/Readout Time Ratio	35
Appendix E. SPICE Simulations	41
Appendix F. Multispectral Radiometer	49

HIGH-SPEED, HIGH-RESOLUTION VIDEO IMAGING SYSTEM

E.L. Dereniak

SCIENTIFIC PERSONNEL

E.L. Dereniak
T. Graeve
L. Flath

OBJECTIVES

Our objectives were to study, design and implement test instrumentation for high-speed imaging devices and instrumentation for obtaining photometric/radiometric data needed to evaluate the in-flight performance of such devices.

RESEARCH FINDINGS

1000³ Imaging System Study

This part of the project involved the study of strategy and specifications for a ruggedized 1000-frame-per-second, airborne qualified, megapixel (1024-by-1024) imager and support system. The initial effort of our research on high speed visible solid state detectors was to theoretically address the radiometric aspects of the problem to estimate the performance of a particular technology configuration with varying figures of merit.

In our initial investigation we used a radiometer, a filter and some targets to substantiate our theory with experimental data. The supporting calculations and the results are shown in Appendix A. The solar constant, as well as radiometric-to-photometric conversion factors were calculated for various spectral bands. The filter used in the experiment transmitted from 0.36 μm to 0.66 μm . The projected signal values for this spectral band, given a standard CCD imager of (10 μm)² pixel size, 25% quantum efficiency and 1 ms integration time, range from 10⁵ to 10⁶ electrons/pixel for scenes illuminated by direct sunlight. Appendix A charts measured vs. calculated irradiance, using standard reflectance values for some of the measured targets. The close agreement between the measured and expected values confirms our model.

Next, we analyzed the signal-to-noise characteristics of a standard CCD imager. The data and calculations are shown in Appendix B. As is evident from the plots, signal-to-noise ratios of 10 and greater can be easily achieved for a variety of signal and read noise values.

Appendix C shows the results of the power dissipation study for a frame transfer CCD. The array modeled is the Ford Aerospace F1024B 1024² pixel imager. Most of the power in the array is generated by capacitive charging and discharging of the clock lines. Using our model, the total power dissipated by this array running at 1000 frames per second was estimated at approximately 10.5 watts. This shows the need for reducing the line-to-line capacitance in the polysilicon clock lines, and maybe even strapping the clock lines using aluminum strips to bring the clock signal out onto the device. The dissipated power can be reduced to approximately 1 watt just by taking simple measures to decrease the line-to-line capacitance.

We performed additional modeling on the effects of the frame-transfer process on image contrast. During readout, each pixel collects additional charges as it is moved across the device. These charges reduce the contrast in the image by averaging or smoothing the pixel contents in the readout direction. For a full frame architecture device, this can lead to a contrast reduction of 50%. In a frame transfer device, a contrast of around 90% can be expected. In an interline sensor, this effect is negligible. The calculations and results are given in Appendix D.

Finally, we modeled the Ford F1024B device on SPICE to determine the clock pulse degradation due to the polysilicon resistance for high frame rates. The model showed significant exponential rise and decay effects on the pulse shape at the center of an array clock line. These effects are due to the combination of the poly line resistance and the large capacitances between the clock line, adjacent lines and the substrate. The maximum working array clock speed for the F1024B device is 500 kHz. The plots shown in Appendix E further explain the model used and the resulting pulse shape degradation.

Airborne Multispectral Radiometer

As part of the effort to further analyze the working environment of a 1000³ imaging system, we designed, built and tested an airborne multispectral radiometer. The primary function of this instrument is to measure radiation reflected off an airplane in several different spectral bands. These data then will be used to develop exact specifications for a high-speed, high-resolution imaging system recording a similar scene.

The system is based around the Xybion MSC-02 Multispectral Video Camera manufactured by Xybion Electronic Systems of San Diego, California. The camera uses a Sony interline transfer CCD with 786 (H)-by-493 (V) pixels and 8.8 mm-by-6.6 mm imaging area. The CCD is located behind a rotating filter wheel equipped with six narrow bandpass interference filters centered at 400 nm, 450 nm, 500 nm, 600 nm, 700 nm and 800 nm. The filter wheel rotates at 600 rpm and is synchronized with the RS-170 video output, so that each consecutive video field corresponds to a different spectral band.

The Xybion camera has been modified to include two photodiodes mounted behind the filter wheel at 120° to the CCD. The field of view of one of the photodiodes has been matched to that of the camera, whereas the other photodiode has an extremely narrow field of view for spot radiometry. The signals from the photodiodes are processed and converted into digital format using two pairs of logarithmic amplifiers and 16-bit A/D converters, and then time-delayed for a fixed number of fields to account for the spectral offset between the photodiode data and the camera video output. The data then are ready to be sent out via the parallel interface to the Video Data Encoder (manufactured by Datum Inc. of Anaheim, California) which inserts it into the current video field.

The multispectral radiometer/camera is mounted inside a heavy-duty aluminum chassis that is designed to withstand the harsh conditions of external mounting on an aircraft. This chassis was designed at the University of Arizona and was built at Eglin Air Force Base under the supervision of D. Snyder and H. McCormick. It includes a power supply, custom electronics, the Xybion camera, and the optics for the radiometers and the camera. A limited amount of space is available for additional cameras. The unit is sealed against the environment with cork gaskets, but there are valves mounted in the front cover plate to equalize pressure differentials between the inside of the box and the outside air as the aircraft changes altitudes. All electrical connectors are easily accessible on top in the rear cover plate. Appendix F shows a sketch of the multispectral radiometer/camera, as well as a diagram of the filter wheel and a list of the system specifications.

High-Speed, High-Resolution CCD Test Station

To evaluate CCD imagers developed for use in the 1000³ imaging system described above, a high-speed focal plane array test station was built. This test station consists of a HP Vectra 486 computer for waveform generation, data acquisition and data analysis/display, as well as custom-built hardware for addressing the FPA and reading out the data. The system is capable of running

multi-channel arrays (up to 64 output channels) at pixel rates up to one MHz. Figure 1 shows a block diagram of the facility.

The custom hardware necessary to operate the test station consists of clock drivers, bias regulators, pre-amps, a 64-channel multiplexer and a correlated double sampling (CDS) unit. It has been optimized for running the Ford Aerospace F1024B CCD. The clock driver and bias regulator hardware is capable of separately adjusting the active area, storage area and serial register clock levels between -10 volts and +10 volts. The DC bias levels can be adjusted between -35 volts and +35 volts. For output signal processing, 12 boards containing 64 pre-amps have been designed, assembled and tested. The 64-channel multiplexer card with built-in gain and offset controls is used to switch the 64 video signals into one single channel. Finally, the CDS unit processes the video signal and reduces noise introduced by capacitive elements in the circuit. It also includes the necessary control circuits for fine-tuning the timing pulses for sampling and A/D conversion.

The test head for the focal plane array consists of a four-layer PCB holding a pin grid array socket into which the 117-pin chip carrier for the CCD is inserted. The PCB is mounted inside a sealed chamber on top of a 5-watt thermoelectric cooler. The chamber can be evacuated to eliminate condensation of moisture on the cooled device. Electrical connections for inputs and outputs to the device are made through three 32-pin sealed Bendix connectors. The test chamber cover includes a 2-in window and an adjustable-focus C-mount lens holder. Three thermistors are mounted inside the test chamber for temperature monitoring.

Several pieces of software have been developed for the test station. The clock waveforms are generated by a data generator board plugged into the computer bus. It has been programmed to run the test array in frame-transfer mode at speeds ranging from <1 frame per second (fps) up to 100 fps. Most of the testing has been performed at either 6 fps or 30 fps.

A 1 MHz ADC board is used to acquire the data presented by the CDS unit. Software has been written both to acquire and display single-channel data and 64-channel composite imagery. In single-channel mode, the test station retrieves data only from one of the 64 channels of the device and displays it on the screen. In 64-channel mode, the acquisition hardware automatically switches to the next channel after every frame, thus assembling a complete 512-by-1024 pixel image in 64 frames. Both modes feature a real-time display with 256 grey levels.

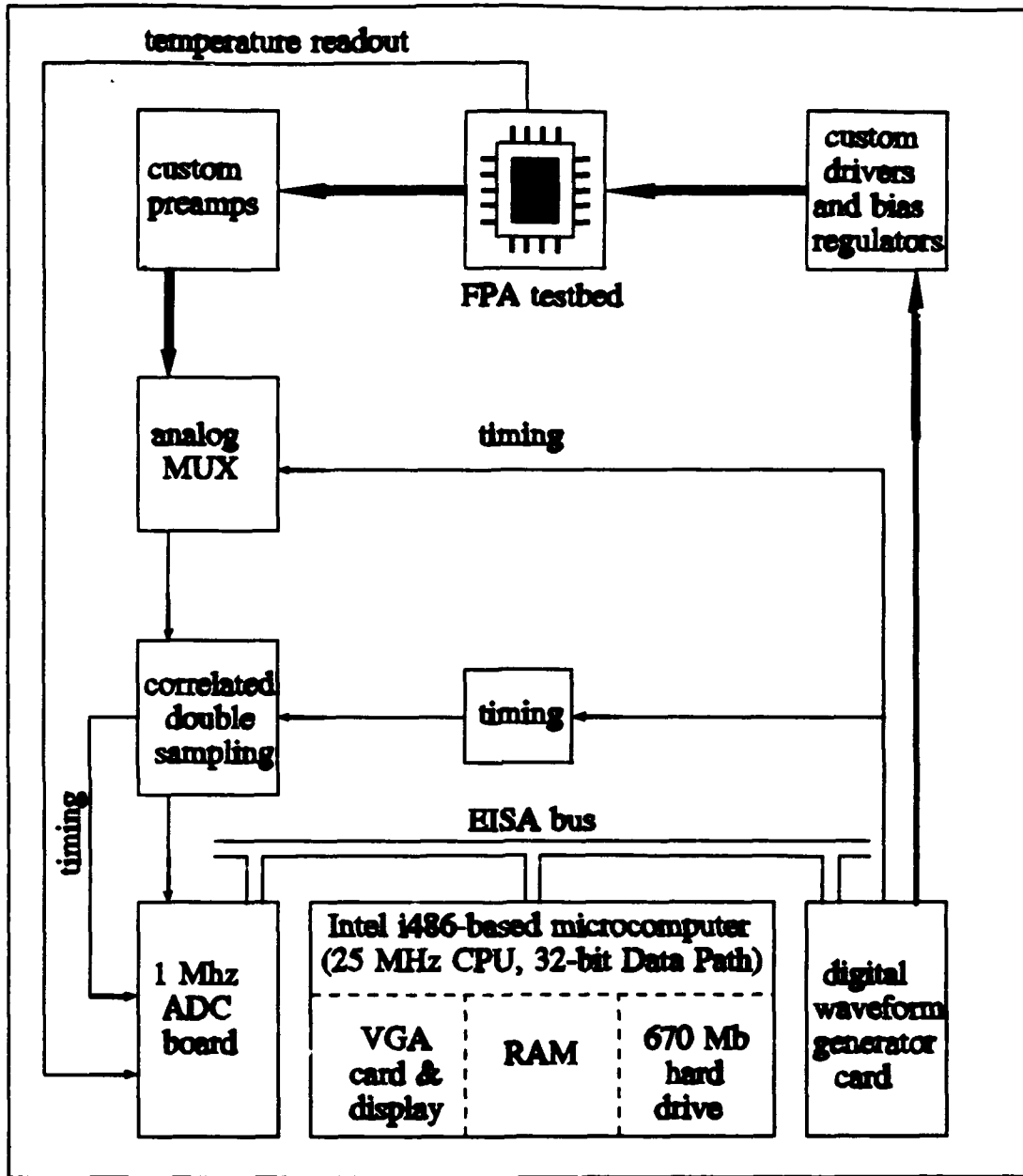


Figure 1. Block diagram of 100 fps test station.

RESULTS AND RECOMMENDATIONS

Test procedures to conduct mean-variance analysis, quantum efficiency, charge-transfer efficiency and MTF tests have been studied. Both software and hardware to conduct automated mean-variance testing has been developed. The results for the mean-variance tests thus far have been limited by a very high read noise level in the acquired data (on the order of 1000 electrons). This is expected to decrease as the electronics are further refined. The mean-variance analysis is further complicated by the fact that the conversion gain in the system is kept low to stay within the voltage swing of the electronics. This leads to a low conversion gain, which makes the mean-variance curve difficult to interpret.

The large voltage swing in the output signal is caused by a DC offset of several volts between the reset and the signal levels in the waveform coming out of the device. This DC offset is caused by capacitive effects as the floating diffusion on the chip is released from the reset potential. The DC offset falls on top of the signal since the reset clock also transfers the signal charge into the floating diffusion. An additional output transfer clock on the device would eliminate this problem by providing an intermediate sampling level to be used as a reference in the correlated double sampling circuit. The electronics could then be tuned to amplify the actual signal and ignore the DC offset.

Another aspect of the device that has been studied is the variation in signal between different outputs on the array. Both shifts in the DC offset described above and in output sensitivity have been observed. The output sensitivity drops by up to three orders of magnitude towards the center of the device. Outputs at the edge of the device are most sensitive and those at the center of the array have the least sensitivity. Further study is necessary to find the exact cause of this effect, but it is believed to be related to a degradation in clock or bias voltages towards the center regions of the CCD. To counteract the signal variations, a two-point software correction scheme has been implemented to equalize differences in both offset and gain between the channels. However, the magnitude of the variations exceeds the range of the A/D converter used for the data acquisition. The correction should be performed in hardware on the analog signal to work satisfactorily.

VACUUM MIRROR STUDIES

W.L. Wolfe

SCIENTIFIC PERSONNEL

W.L. Wolfe

L. Brod

D. Eklund

V. Sinclair

OBJECTIVES

Our objectives were to study thin-film mirrors, under vacuum, whose properties have been directionally altered by x-rays or other means.

RESEARCH FINDINGS

Our collaborator, Dr. William Gamble of the U.S. Army MICOM, suggested that a very effective optical system for missile guidance applications would be one made of thin films of mylar or similar materials. Such a mirror or system of mirrors provide a lightweight, inexpensive optical element or system of elements and it has the potential for simple refocussing. By simply changing the pressure on the system, one could change the curvature of the mirror. Other possibilities for shaping the mirror exist. For example, the membrane could be made aspherical through local alteration of its chemical or physical structure. These techniques seemed to hold great promise, so an exploratory program was undertaken. This program included the preliminary formation of mirrors, design considerations, and prescriptions for a Fresnel mirror to ameliorate certain difficulties.

The first stage of the research program comprised an extensive literature search, because it seemed likely that this concept would have been investigated previously. Such was the case, but unfortunately, no articles were pertinent. Applications were for radar and solar energy, neither which require the surface perfection required by visible or infrared optical systems. Therefore, we were on our own. We continued communications with Dr. Gamble who had carried out other exploratory investigations.

Original tests showed that reflectorized mylar can be formed in reasonable concave and convex figures. Pressures ranged near atmospheric -- approximately 10% above or below one atmosphere would produce curvatures that can be described as about F/5. Tests were made with a 2-in diameter ring of mylar. Higher speeds and lower F/numbers introduced "wrinkling" at the mirror edges.

This is not unexpected, because the surface is being distorted from a plane to an approximate sphere. The wrinkling is a function of membrane elasticity. It appears that to obtain very fast optics will require surfaces of the approximate final shape or an equivalent technique.

From results of the first set of experiments, and through further discussions with Dr. Gamble, we designed a Fresnel version of such a system. The Fresnel mirror is of the same configuration as a Fresnel lens, a stepped approximation to the curvature desired. The system was designed so that imaging experiments can be carried out with a helium-neon laser. The steps, therefore, must be in half-multiples of $0.6328 \mu\text{m}$. The membrane can be no thicker than 0.005 in ($\sim 125 \mu\text{m}$). The diameter is assumed to be 2 in ($\sim 50 \text{ mm}$). An F/3 system would have a focal length of 150 mm and, therefore, a radius of curvature of 300 mm. The sag then is 1.04 mm. Such a system can be realized in 1643 one-wavelength steps or larger. The largest step should probably be about one/tenth the thickness of the material, or about $12.5 \mu\text{m}$, giving ten steps across the material. A reasonable compromise is 20 radial steps, each of about 0.1 mm. In fact, each step will be 158 wavelengths, or $99.97 \mu\text{m}$, a reasonable step height. If the height is too shallow, the unavoidable rounding of the corners has a deleterious effect on the operation of the Fresnel element.

PLANS

The Fresnel master has been ordered from the University of Alabama, Huntsville, and will be delivered to Dr. Gamble.

APPENDIX A
RADIOMETRIC CALCULATIONS AND
MEASUREMENTS

SOLAR CONSTANT – JUSTIFICATION OF METHODS

1. Radiant Exitance of sun in visible spectrum, from Planck's equation, assuming it to be a perfect black body at 5900 K:

$$M = \int_{.4}^{.76} \frac{3.7415 \cdot 10^4}{\lambda^5 \left[\exp \left[\frac{14388}{\lambda \cdot 5900} \right] - 1 \right]} d\lambda$$

$$M = 2.95 \cdot 10^3 \text{ Watts/cm}^2$$

2. Radiance of sun, assuming that it is a Lambertian source:

$$L = \frac{M}{\pi} \quad L = 940 \text{ Watts/cm}^2/\text{sr}$$

3. Solid angle subtended by sun as seen from earth:

$$\text{radius of sun} \quad r = 6.95 \cdot 10^{10} \text{ cm}$$

$$\text{distance earth-to-sun} \quad d = 1.5 \cdot 10^{13} \text{ cm}$$

$$\Omega = \frac{\pi r^2}{d^2} \quad \Omega = 6.7 \cdot 10^{-5} \text{ sr}$$

4. Irradiance incident on earth's atmosphere:

$$E = L\Omega \quad E = 0.063 \text{ Watts/cm}^2$$

$$E \cdot 10^4 = 634 \text{ Watts/m}^2$$

5. For comparison, assuming that 46% of solar energy falls in the visible band, the solar constant is:

$$0.46 \cdot 1360 = 626 \text{ Watts/m}^2$$

Conclusion: The irradiance incident on earth's atmosphere as derived from our radiometric model is virtually identical to the value given for the solar constant in the *Manual of Remote Sensing*.

Note: 35.3% of solar energy falls in .38 to .66 μm band.

ADJUSTED SOLAR CONSTANT AND FILTER TRANSMISSION

Planck Equation for Black Body Radiant Exitance of sun:

$$M(\lambda) = 37418 \cdot \lambda^{-5} \left[\exp\left[\frac{14388}{\lambda \cdot 5900}\right] - 1 \right]^{-1} \quad (\text{in Watts/cm}^2/\mu\text{m})$$

Curve Fit for CS 1-56 infrared blocking filter:

$$\begin{aligned} A0 &:= -23807.4 & A1 &:= 276308 \\ A2 &:= -1335780 & A3 &:= 3436050 \\ A4 &:= -4947200 & A5 &:= 3774250 \\ A6 &:= -1191400 \end{aligned}$$

$$f(\lambda) = 0.01 \cdot [A0 + A1\lambda + A2\lambda^2 + A3\lambda^3 + A4\lambda^4 + A5\lambda^5 + A6\lambda^6] \quad (\% \text{ transmission})$$

1. Calculated Solar Constant at sea level, adjusted for transmission band of filter:

$$E1 = 0.83 \cdot 6.7 \cdot 10^{-5} \cdot \frac{1}{\pi} \cdot \int_{.38}^{.66} M(\lambda) d\lambda$$

$$E1 = 0.043 \text{ Watts/cm}^2$$

2. Average filter transmission (experimental) given by measured value divided by Solar Constant:

$$T1 = \frac{0.011}{E1} \cdot 100 \quad T1 = 25.7\%$$

3. Calculated Solar Constant at sea level, adjusted for spectral transmission of filter:

$$E2 = 0.83 \cdot 6.7 \cdot 10^{-5} \cdot \frac{1}{\pi} \cdot \int_{.38}^{.66} f(\lambda) \cdot M(\lambda) d\lambda$$

$$E2 = 0.012 \text{ Watts/cm}^2$$

4. Average filter transmission (calculated) given by ratio of Solar Constants from parts 1 and 3:

$$T2 = \frac{E2}{E1} \cdot 100 \quad T2 = 28.5\%$$

WATTS TO PHOTONS/SEC CONVERSION FACTOR

Radiant Exitance of sun over filter transmission band:

$$M_e = \int_{.38}^{.66} \frac{3.7415 \cdot 10^4}{\lambda^5 \left[\exp \left[\frac{14388}{\lambda \cdot 5900} \right] - 1 \right]} d\lambda \quad (\text{in Watts/cm}^2)$$

Photon-Flux Exitance of sun over filter transmission band:

$$M_p = \int_{.38}^{.66} \frac{1.885 \cdot 10^{23}}{\lambda^4 \left[\exp \left[\frac{14388}{\lambda \cdot 5900} \right] - 1 \right]} d\lambda \quad (\text{in Photons/sec/cm}^2)$$

Conversion Factor (Watts to Photons/sec):

$$F = \frac{M_p}{M_e} = 2.612 \cdot 10^{18} \quad \text{Photons/sec/Watt}$$

WATTS/CM² TO LUX CONVERSION FACTOR

Planck Equation for Black Body Radiant Exitance of sun:

$$M(\lambda) = 37415 \cdot \lambda^{-5} \left[\exp\left[\frac{14388}{\lambda \cdot 5900}\right] - 1 \right]^{-1} \text{ (in Watts/cm}^2/\mu\text{m)}$$

Curve Fit for photopic response curve:

$$v(\lambda) = 1.0185 \exp[-285.53 (\lambda - .56017)^2] \text{ (rel. response)}$$

Radiant Exitance of sun over filter transmission band:

$$M_r = \int_{.38}^{.66} M(\lambda) d\lambda \text{ (in Watts/cm}^2\text{)}$$

Luminous Exitance of sun over filter transmission band:

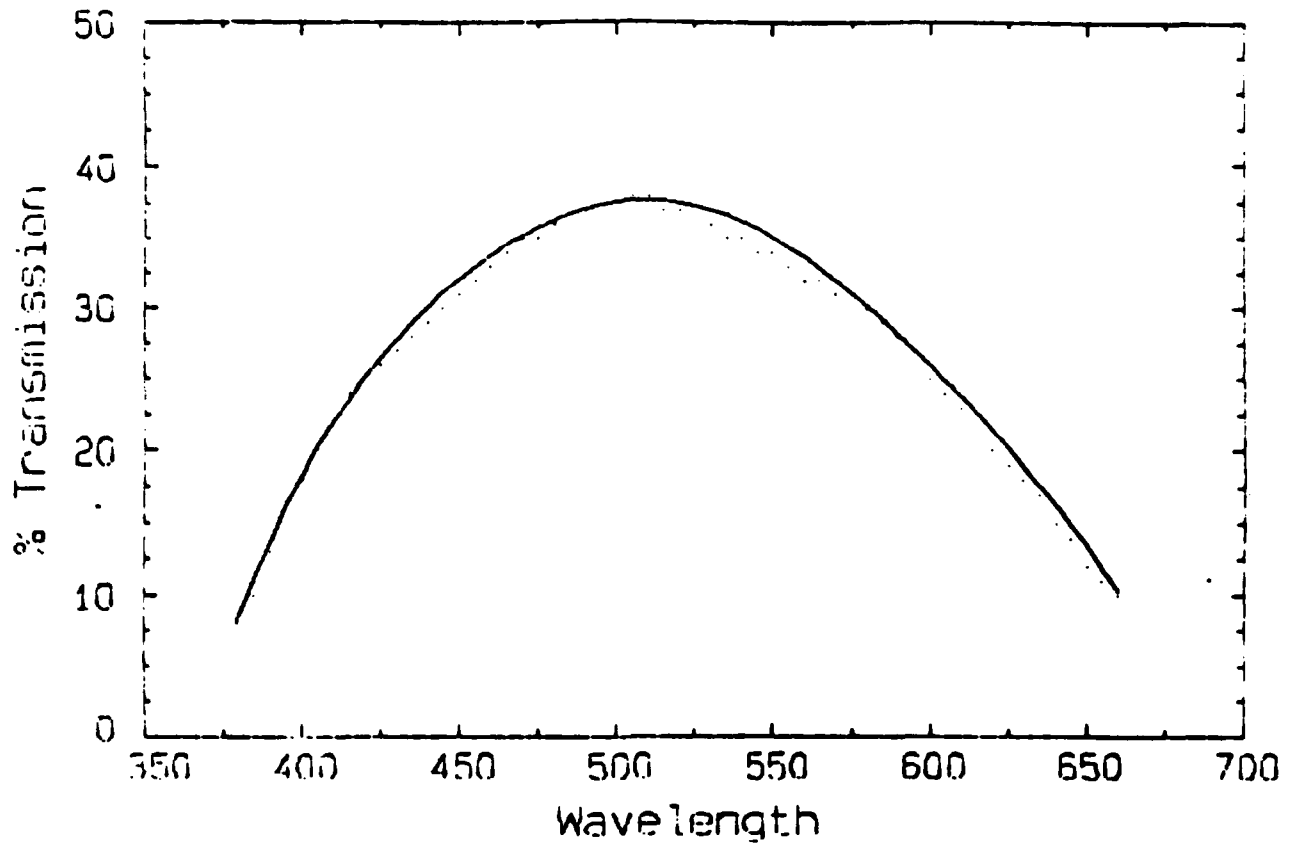
$$M_v = 683 \cdot \int_{.38}^{.66} v(\lambda) M(\lambda) d\lambda \text{ (in Lumen/cm}^2\text{)}$$

Conversion Factor (Watts to Lumen or Watts/m² to Lux):

$$F = \frac{M_v}{M_r} = 262 \text{ Lumen/Watt or Lux/Watt/m}^2$$

$$10^4 \cdot \frac{M_v}{M_r} = 2.62 \cdot 10^6 \text{ Lux/Watt/cm}^2$$

CS 1-56 Infrared Blocking Filter



CONVERSION FACTOR: CD/M² TO PHOTONS/SEC-CM²-SR

(sunlight only – 450 nm to 950 nm band)

Planck Equation for Black Body Photon-Flux Exitance of sun:

$$M_p(\lambda) = 1.885 \cdot 10^{23} \cdot \lambda^{-4} \left[\exp \left[\frac{14388}{\lambda \cdot 5900} \right] - 1 \right]^{-1} \text{ (in photons/sec-cm}^2/\mu\text{m)}$$

Planck Equation for Black Body Radiant Exitance of sun:

$$M_e(\lambda) = 37415 \cdot \lambda^{-5} \left[\exp \left[\frac{14388}{\lambda \cdot 5900} \right] - 1 \right]^{-1} \text{ (in Watts/cm}^2\mu\text{m)}$$

Curve Fit for photopic response curve:

$$v(\lambda) = 1.0185 \exp \left[-285.53 \cdot (\lambda - .56017)^2 \right] \text{ (rel. response)}$$

Photon-Flux Radiance of sun over 450 - 950 nm band:

$$L_p = \frac{1}{\pi} \left[\int_{.45}^{.95} M_p(\lambda) d\lambda \right] \text{ (in photons/sec-cm}^2\text{-sr)}$$

Luminance of sun:

$$L_v = \frac{1}{\pi} \cdot 683 \cdot \int_{.45}^{.95} v(\lambda) M_e(\lambda) d\lambda \text{ (in Cd/cm}^2\text{)}$$

Conversion Factor (Cd/m² to Photons/sec-cm²-sr):

$$F = \frac{L_p}{L_v} \cdot 10^{-4} = 1.83 \cdot 10^{12} \text{ Photons/sec-cm}^2\text{-sr/Cd/m}^2$$

CONVERSION FACTOR: CD/M² TO PHOTONS/SEC-CM²-SR

(sunlight only – 450 nm to 800 nm band)

Planck Equation for Black Body Photon-Flux Exitance of sun:

$$M_p(\lambda) = 1.885 \cdot 10^{23} \cdot \lambda^{-4} \left[\exp\left[\frac{14388}{\lambda \cdot 5900}\right] - 1 \right]^{-1} \text{ (in photons/sec-cm}^2/\mu\text{m)}$$

Planck Equation for Black Body Radiant Exitance of sun:

$$M_r(\lambda) = 37415 \cdot \lambda^{-5} \left[\exp\left[\frac{14388}{\lambda \cdot 5900}\right] - 1 \right]^{-1} \text{ (in Watts/cm}^2/\mu\text{m)}$$

Curve Fit for photopic response curve:

$$v(\lambda) = 1.0185 \exp[-285.53 \cdot (\lambda - .56017)^2] \text{ (rel. response)}$$

Photon-Flux Radiance of sun over 450 - 800 nm band:

$$L_p = \frac{1}{\pi} \left[\int_{.45}^{.80} M_p(\lambda) d\lambda \right] \text{ (in photons/sec-cm}^2\text{-sr)}$$

Luminance of sun:

$$L_v = \frac{1}{\pi} \cdot 683 \cdot \int_{.45}^{.80} v(\lambda) M_r(\lambda) d\lambda \text{ (in Cd/cm}^2\text{)}$$

Conversion Factor (Cd/m² to Photons/sec-cm²-sr):

$$F = \frac{L_p}{L_v} \cdot 10^{-4} = 1.33 \cdot 10^{12} \text{ Photons/sec-cm}^2\text{-sr/Cd/m}^2$$

CONVERSION FACTOR: CD/M² TO PHOTONS/SEC-CM²-SR

(sunlight only – 450 nm to 670 nm band)

Planck Equation for Black Body Photon-Flux Exitance of sun:

$$M_p(\lambda) = 1.885 \cdot 10^{23} \cdot \lambda^{-4} \left[\exp\left[\frac{14388}{\lambda \cdot 5900}\right] - 1 \right]^{-1} \text{ (in photons/sec/cm}^2\text{/}\mu\text{m)}$$

Planck Equation for Black Body Radiant Exitance of sun:

$$M_e(\lambda) = 37415 \cdot \lambda^{-5} \left[\exp\left[\frac{14388}{\lambda \cdot 5900}\right] - 1 \right]^{-1} \text{ (in Watts/cm}^2\text{/}\mu\text{m)}$$

Curve Fit for photopic response curve:

$$v(\lambda) = 1.0185 \exp[-285.53 \cdot (\lambda - .56017)^2] \text{ (rel. response)}$$

Photon-Flux Radiance of sun over 450 - 670 nm band:

$$L_p = \frac{1}{\pi} \left[\int_{.45}^{.67} M_p(\lambda) d\lambda \right] \text{ (in photons/sec-cm}^2\text{-sr)}$$

Luminance of sun:

$$L_v = \frac{1}{\pi} \cdot 683 \cdot \int_{.45}^{.67} v(\lambda) M_e(\lambda) d\lambda \text{ (in Cd/cm}^2\text{)}$$

Conversion Factor (Cd/m² to Photons/sec-cm²-sr):

$$F = \frac{L_p}{L_v} \cdot 10^{-4} = 8.41 \cdot 10^{11} \text{ Photons/sec-cm}^2\text{-sr/Cd/m}^2$$

CONVERSION FACTOR: CD/M² TO WATTS/CM²-SR

(sunlight only – 450 nm to 950 nm band)

Planck Equation for Black Body Radiant Exitance of sun:

$$M(\lambda) = 37415 \cdot \lambda^{-5} \left[\exp\left[\frac{14388}{\lambda \cdot 5900}\right] - 1 \right]^{-1} \text{ (in Watts/cm}^2\text{/}\mu\text{m)}$$

Curve Fit for photopic response curve:

$$v(\lambda) = 1.0185 \exp[-285.53 \cdot (\lambda - .56017)^2] \text{ (rel. response)}$$

Radiance of sun over 450 - 950 nm band:

$$L_e = \frac{1}{\pi} \left[\int_{.45}^{.95} M(\lambda) d\lambda \right] \text{ (in Watts/cm}^2\text{-sr)}$$

Luminance of sun:

$$L_v = \frac{1}{\pi} \cdot 683 \cdot \int_{.45}^{.95} v(\lambda) M(\lambda) d\lambda \text{ (in Cd/cm}^2\text{)}$$

Conversion Factor (Cd/m² to Watts/cm²-sr):

$$F = \frac{L_e}{L_v} \cdot 10^{-4} = 5.47 \cdot 10^{-7} \text{ Watts/cm}^2\text{-sr/Cd/m}^2$$

CONVERSION FACTOR: CD/M² TO WATTS/CM²-SR

(sunlight only – 450 nm to 800 nm band)

Planck Equation for Black Body Radiant Exitance of sun:

$$M(\lambda) = 37415 \cdot \lambda^{-5} \left[\exp\left[\frac{14388}{\lambda \cdot 5900}\right] - 1 \right]^{-1} \text{ (in Watts/cm}^2\text{/}\mu\text{m)}$$

Curve Fit for photopic response curve:

$$v(\lambda) = 1.0185 \cdot \exp[-285.53 \cdot (\lambda - .56017)^2] \text{ (rel. response)}$$

Radiance of sun over 450 - 800 nm band:

$$L_e = \frac{1}{\pi} \left[\int_{.45}^{.80} M(\lambda) d\lambda \right] \text{ (in Watts/cm}^2\text{-sr)}$$

Luminance of sun:

$$L_v = \frac{1}{\pi} \cdot 683 \cdot \int_{.45}^{.80} v(\lambda) \cdot M(\lambda) d\lambda \text{ (in Cd/cm}^2\text{)}$$

Conversion Factor (Cd/m² to Watts/cm²-sr):

$$F = \frac{L_e}{L_v} \cdot 10^{-4} = 4.33 \cdot 10^{-7} \text{ Watts/cm}^2\text{-sr/Cd/m}^2$$

CONVERSION FACTOR: CD/M² TO WATTS/CM²-SR

(sunlight only – 450 nm to 670 nm band)

Planck Equation for Black Body Radiant Exitance of sun:

$$M(\lambda) = 37415 \cdot \lambda^{-5} \left[\exp\left[\frac{14388}{\lambda \cdot 5900}\right] - 1 \right]^{-1} \text{ (in Watts/cm}^2\text{/}\mu\text{m)}$$

Curve Fit for photopic response curve:

$$v(\lambda) = 1.0185 \exp[-285.53 \cdot (\lambda - .56017)^2] \text{ (rel. response)}$$

Radiance of sun over 450 - 670 nm band:

$$L_s = \frac{1}{\pi} \cdot \int_{.45}^{.67} M(\lambda) d\lambda \text{ (in Watts/cm}^2\text{-sr)}$$

Luminance of sun:

$$L_v = \frac{1}{\pi} \cdot 683 \cdot \int_{.45}^{.67} v(\lambda) M(\lambda) d\lambda \text{ (in Cd/cm}^2\text{)}$$

Conversion Factor (Cd/m² to Watts/cm²-sr):

$$F = \frac{L_s}{L_v} \cdot 10^{-4} = 3 \cdot 10^{-7} \text{ Watts/cm}^2\text{-sr/Cd/m}^2$$

ESTIMATED SIGNAL FOR MEASURED TARGET RADIANCES

Object (in full sunlight)	Measured Value (E) (mW/cm ²)	Actual Value (E') (mW/cm ²)	Target Radiance (L) (mW/cm ² /sr)	Irrad. on FPA (E _d) (mW/cm ²)	Phot. Flux Density (E _p) (photons/ sec-cm ²)	Signal (S) (electrons)
Black Roof	0.065	0.232	1.085	0.192	5.02E+14	1.25E+05
Red Brick	0.100	0.357	1.669	0.295	7.72E+14	1.93E+05
Dull Aluminum	0.150	0.536	2.503	0.443	1.16E+15	2.89E+05
Concrete	0.270	0.964	4.506	0.798	2.08E+15	5.21E+05
White Roof	0.290	1.036	4.840	0.857	2.24E+15	5.59E+05
Shiny Aluminum	0.600	2.143	10.013	1.772	4.63E+15	1.16E+06

E = Irradiance on radiometer head (target filling entire field of view)

$E' = E/0.28$ = Irradiance on radiometer head adjusted for average filter transmission

$L = E'/0.214$ = Target Radiance (0.214 = solid angle subtended by target = field of view of radiometer head)

$E_d = (\pi/4) \cdot 0.90/(F/\#)^2 \cdot L$ = calculated Irradiance on Focal Plane, assuming F/2 lens with 90% transmission

$E_p = 2.612 \cdot 10^{15} \cdot E_d$ = equivalent Photon Flux Density incident on Focal Plane, adjusted for transmission band of filter

$S = \eta \cdot t \cdot A \cdot E_p$ = number of electrons generated in well, assuming a Quantum Efficiency (η) of 25%, integration time (t) of 1 ms and active pixel area (A) of $(10 \mu\text{m})^2$

MEASURED VS. EXPECTED IRRADIANCE VALUES

Material (in full sunlight)	Reflectance (ρ)	Measured Irradiance (E_m) (mW/cm ²)	Expected Irradiance (E_e) (mW/cm ²)
Black roof	10%	0.065	0.075
Concrete	35%	0.270	0.262
Aluminum	90%	0.600	0.674

$$E_e = E_s / \pi \cdot \rho \cdot \Omega$$

where E_s = measured solar constant (11 mW/cm²)
 ρ = reflectance of material (rough estimate based on graphs in IR Handbook)
 Ω = solid angle of field-of-view of radiometer (0.214 sr)

APPENDIX B
EXPECTED SIGNAL-TO-NOISE RATIO

EXPECTED SIGNAL-TO-NOISE RATIO

- Signal values are expected to vary between 1E3 and 1E6 electrons (see Appendix A).
- Noise sources are photon, read and dark current noise.

- Photon noise: $np(S) = \sqrt{S}$

- Read noise: $nr = 100$

- Dark current noise:

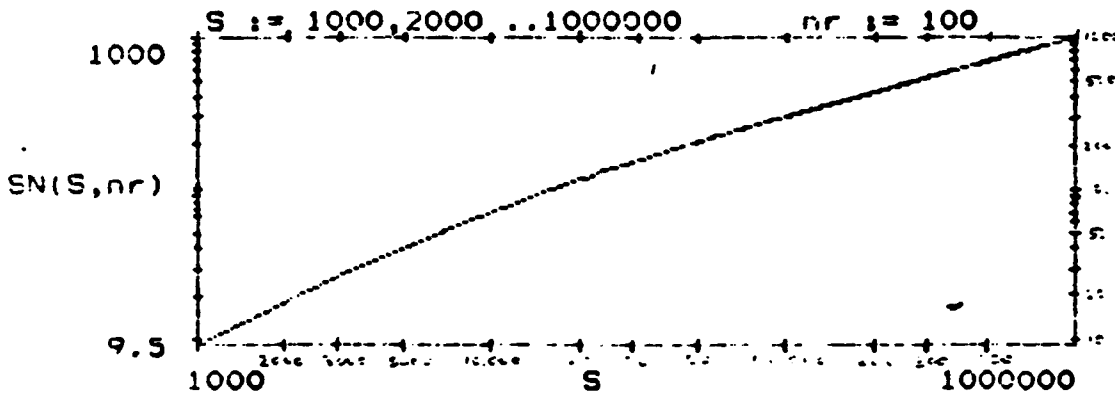
active area	$A = 2.25 \cdot 10^{-6} \text{ cm}^2$
integration time	$t = 0.001 \text{ sec}$
	$q = 1.6 \cdot 10^{-19} \text{ Coul.}$
dark current	$Jd: 10^9 \text{ A/cm}^2 \text{ at } 300 \text{ }^\circ\text{K}$

$$nd = \sqrt{\frac{Jd \cdot A \cdot t}{q}} \quad nd = 3.75$$

- Signal-to-Noise ratio:

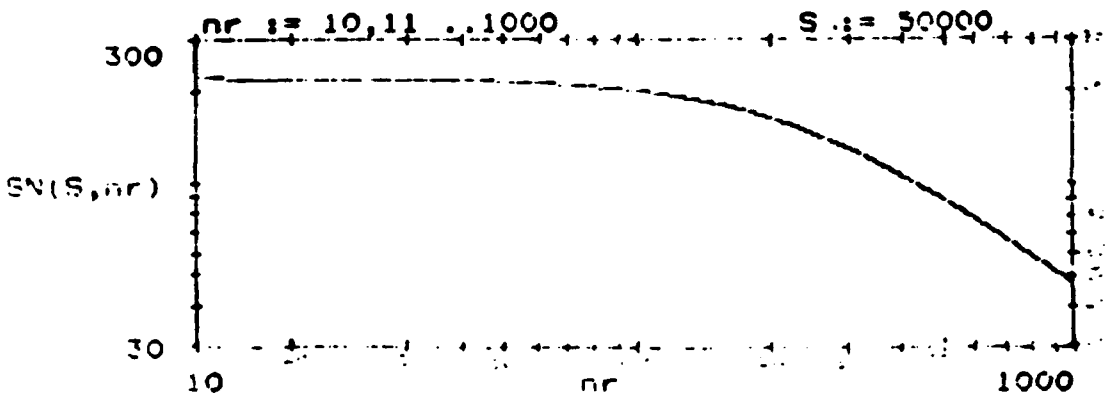
$$SN(S, nr) = \frac{S}{\sqrt{np(s)^2 + nr^2 + nd^2}}$$

- S/N vs. signal (log/log):



- S/N vs. read noise (log/log):

- S/N vs. read noise (log/log):



APPENDIX C
POWER DISSIPATION

Power Dissipation

The power dissipation on a focal plane array depends on three different processes. Most of the power is generated by capacitive charge and discharge currents running through resistive elements in the device structure. Another significant power source can be the on-chip output amplifiers. The third source of power generation are carrier lift and friction mechanisms as charge packets are moved across the device. All power sources depend on basic material parameters, the device architecture and layout, and the clocking scheme used. The following analysis neglects clock pulse degradation due to lossy clock lines.

As a clock pulse is applied to the device, the oxide and depletion region capacitances in each pixel are charged up. The charge current dissipates energy by flowing through the high-resistance epitaxial layer into the substrate. For a trapezoidal clock pulse with rise and fall times t_r and voltage differential V_g between the two clock bias levels, the current is approximately constant over the linear voltage ramp and can be expressed as

$$i_{pix} = \frac{C_{pix} V_g}{t_r} .$$

The dissipated power is then given by integrating $i^2 R$ over the period of one clock cycle. Since the current is zero except when the clock voltage is changing, this integral reduces to

$$P_{opi} = \frac{2}{T} \int_0^{t_r} i_{pix}^2 R_{opi} dt ,$$

where T is the period of the clock cycle ($T=1/f_c$). The factor of two is due to the power being dissipated on both the rising and the falling edge of the clock pulse. To get the total power, P_{opi} has to be multiplied by the number of affected pixels and the duty cycle of the clock waveform. Solving the integral,

$$P_{opi}^T = 2 \Phi N i_{pix}^2 R_{opi} t_r f_c d ,$$

where Φ is the number of phases, N is the number of pixels and d is the duty cycle.

A second source of power dissipation is the resistance of the polysilicon lines. This resistance is encountered as the current charges up the pixel capacitance C_{pix} and the poly-to-poly capacitance C_{poly} . Following the above argument,

$$i_{pix} = \frac{(C_{pix} + 2C_{poly}) V_g}{t_r} .$$

This current has to be summed over half of each 1024-pixel clock line, since each pixel sees a different current. The total power dissipated in the polysilicon clock lines is

$$P_{poly}^T = 4 \Phi N_l \sum_{n=1}^m n^2 i_{pix}^2 R_{poly} t_r f_c d .$$

Here N_l is the number of lines and $\Sigma n^2 = m(m+1)(2m+1)/6$. The additional factor of two is due to the fact that each line is 1024 pixels long and driven on both ends, so that $m=512$.

Power is also generated due to carrier lift and friction as charge packets are transported across the array. This power is given by

$$P_{\text{fric}} = N \frac{qS}{\mu} (Lf_c)^2 d$$

$$P_{\text{lift}} = \Phi N q S f_c \left(V_s - \frac{qS}{2C_{ox}} \right) d .$$

S is the number of electrons in each signal package, L is the pixel length, q the electron charge and μ the carrier mobility.

Finally, power is generated by the 64 output FETs on the chip. Neglecting rise and fall times on the output signal, it is given by

$$P_{\text{FET}} = 64 (V_{OD} - V_o) \left(\frac{V_o}{R_{\text{load}}} \right) d .$$

V_{OD} is the output drain supply voltage, V_o is the output voltage and R_{load} is the load resistance attached to the output amplifier.

These equations can now be evaluated for a given array. In this case the Ford F1024B array running in frame transfer mode at a frame rate of 1000 fps will be used. To calculate the total power, the readout process has to be separated into three sections. First, the charge is transferred from the integration region to the storage region at a clock speed of 1 MHz. This process takes 256 μs . During the remaining 744 μs of the frame period, the 256 lines of data in the storage region are read out into the serial registers at a clock speed of 344 kHz. At the same time, the serial registers are clocking out the charge at 16.8 MHz, running idle for 1 μs every 32 cycles to wait for a new line of data to be transferred from the storage area.

A few special rules apply. The outputs of the device are at a low signal level, corresponding to the full well output, for half the time during which the serial registers are running (0.244 duty cycle). For the remaining time, they are at the reset level V_o' , which is closer to V_{OD} . For the serial readout, the pixel capacitance is doubled and the epi resistance halved since the pixels in the serial readout register have twice the area of the array pixels. Finally, the number of pixels for the active-to-storage area transfer for the power generated by carrier lift and friction is halved since only half the pixels on the array carry charge.

Epitaxial Layer:

	<u>Transfer to Storage Area</u>		<u>Transfer to Serial Register</u>		<u>Serial Register Readout</u>	
Φ	3		3		3	
N	1048576		1048576		2048	
C_{pix}	1.5	fF	1.5	fF	3	fF
R_{epi}	80	k Ω	80	k Ω	40	k Ω
V_g	10	V	10	V	12	V
t_r	100	ns	100	ns	10	ns
f_c	1	MHz	344	kHz	16.8	MHz
d	25.6	%	74.4	%	48.8	%
P_{epi}	290	nWatts	150	nWatts	520	nWatts
total:	960	nWatts				

Polysilicon Lines:

	<u>Transfer to Storage Area</u>		<u>Transfer to Serial Register</u>		<u>Serial Register Readout</u>	
Φ	3		3		3	
N_1	1024		512		2048	
Σn^2	44870400		44870400		1	
C_{pix}	1.5	fF	1.5	fF	3	fF
C_{poly}	10	fF	10	fF	20	fF
R_{poly}	100	Ω	100	Ω	200	Ω
V_g	10	V	10	V	12	V
t_r	100	ns	100	ns	10	ns
f_c	1	MHz	344	kHz	16.8	MHz
d	25.6	%	74.4	%	48.8	%
P_{epi}	6.5	Watts	3.3	Watts	540	μ Watts
total:	9.8	Watts				

Output FETs:

	<u>V_o low</u>		<u>V_o high</u>	
V_{OD}	20	V	20	V
V_o	11	V	12	V
R_{load}	10	k Ω	10	k Ω
d	24.4	%	75.6	%
P_{FET}	160	mWatts	460	mWatts
total:	620	mWatts		

Carrier Lift/Friction:

	<u>Transfer to Storage Area</u>		<u>Transfer to Serial Register</u>		<u>Serial Register Readout</u>	
n	3		3		3	
N	524288		262144		1024	
C_{ox}	26	fF	26	fF	52	fF
S	100000	e^-	100000	e^-	100000	e^-
L	15	μm	15	μm	15	μm
μ	1300	cm^2/Vs	1300	cm^2/Vs	1300	cm^2/Vs
V_g	10	V	10	V	12	V
f_c	1	MHz	344	kHz	16.8	MHz
d	25.6	%	74.4	%	48.8	%
P_{lift}	62	mWatts	31	mWatts	4.8	mWatts
P_{fric}	3.7	μ Watts	0.6	μ Watts	3.9	μ Watts
total:	98	mWatts				

grand total: 10.5 Watts

The total power dissipated by the array in this model is 10.5 Watts. This points out several problems. The main power contribution of 9.8 Watts is generated in the array polysilicon lines due to the extremely high capacitances encountered between adjacent lines. In an actual device, the power dissipation would never reach these levels since the assumption of lossless clock lines does not hold. The clock pulse would be degraded significantly towards the center of a clock line, so that less current is generated and the power dissipation is kept low.

Two solutions exist for this problem. The polysilicon clock lines could be strapped by aluminum lines, which have less resistance and therefore cause less pulse degradation and power generation. However, since the large capacitances remain, this solution would create extremely high currents during the rising and falling edges of the clock pulses. Measures have to be taken to reduce the line-to-line capacitance, either by reducing the overlap area or by increasing the thickness of the oxide insulation in between polysilicon layers. Calculations show that by decreasing the overlap area by half to one micron overlap, and increasing the oxide thickness from 1000 Å to 5000 Å, the overlap capacitance can be reduced to 1 fF. This in turn reduces the total dissipated power to one Watt. The best solution is probably a combination of both aluminum lines to ensure accurate clock pulses and reduced capacitance to reduce high charging currents.

APPENDIX D
CONTRAST DEGRADATION DUE TO
INTEGRATION/READOUT TIME RATIO

Contrast Degradation due to Integration/Readout Time Ratio (T. Graeve)

Let the ratio of integration time to readout time be R (i.e. $R:1$). For a given array size and frame rate, a full frame architecture has the lowest R , a frame transfer device has a higher R , and an interline device has the highest R . However, for the latter there is no degradation in contrast due to charge readout. The following analysis is therefore valid only for full frame and frame transfer devices.

For a normal scene, we define the maximum and minimum irradiance incident on the devices E_{\max} and E_{\min} respectively. The maximum contrast for this scene then becomes

$$C_{\max} = \frac{\eta A_d t_i (E_{\max} - E_{\min})}{\eta A_d t_i (E_{\max} + E_{\min}) + 2 t_i n}$$

where η is the quantum efficiency and A_d the area of the device. During readout, each pixel collects an additional charge proportional to the average irradiance on the column that it is transferred through. If this average irradiance is given by $\alpha \cdot E_{\max}$, where α is a factor between zero and one and the readout time is t_i/R , the minimum and maximum signal levels are

$$S_{\min} = \eta A_d t_i E_{\min} + t_i \left(1 + \frac{1}{R}\right) n + \eta A_d \frac{t_i}{R} \alpha E_{\max}$$

$$S_{\max} = \eta A_d t_i E_{\max} + t_i \left(1 + \frac{1}{R}\right) n + \eta A_d \frac{t_i}{R} \alpha E_{\max}$$

The actual contrast then becomes

$$C_{act} = \frac{\eta A_d [E_{\max} - E_{\min}]}{\eta A_d \left[\left(1 + \frac{2\alpha}{R}\right) E_{\max} + E_{\min} \right] + 2 \left(1 + \frac{1}{R}\right) n}$$

For an E_{\min} of zero and no dark current, this equation reduces to

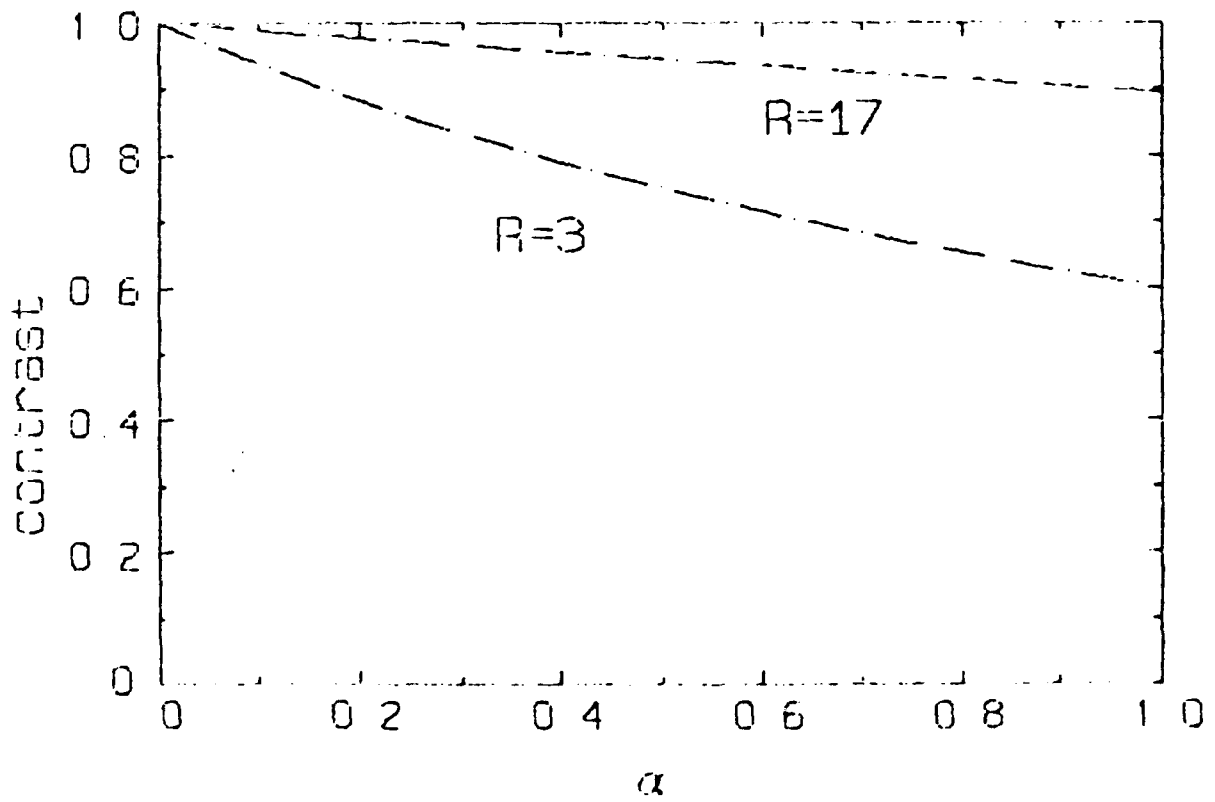
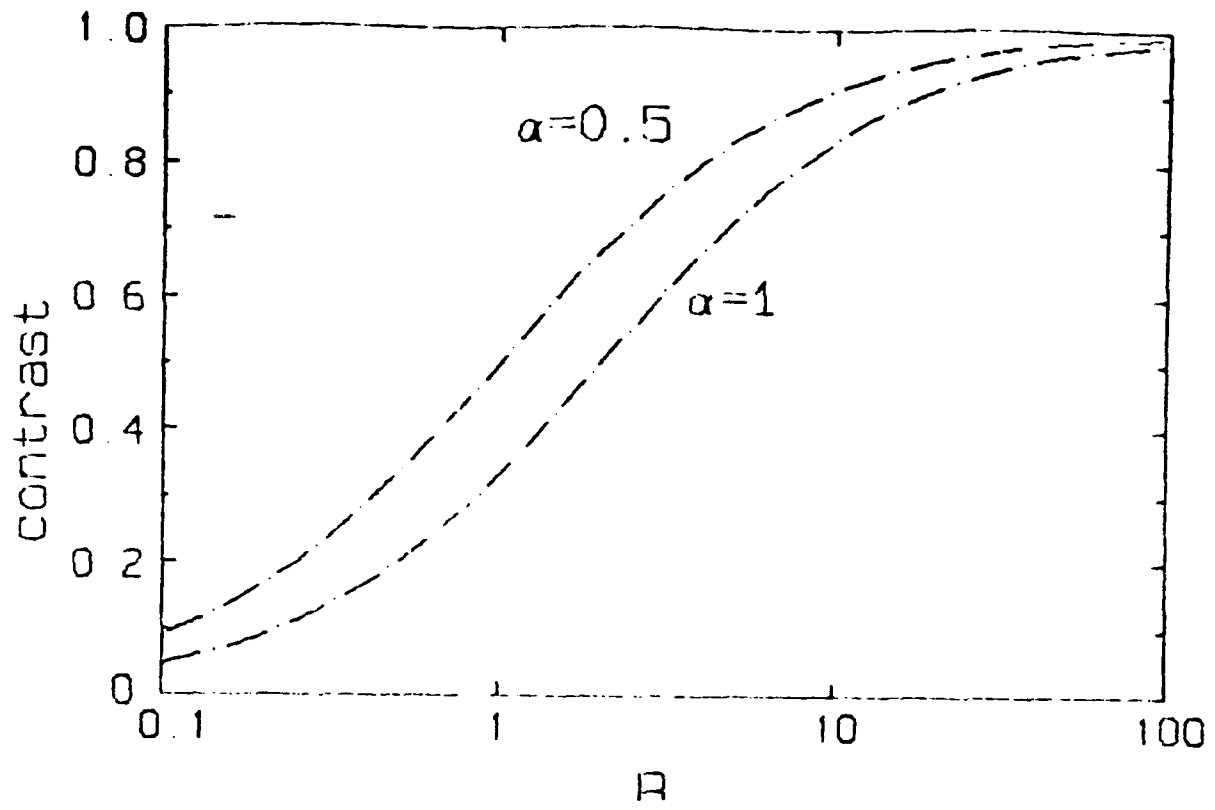
$$C_{act} = \frac{1}{1 + \frac{2\alpha}{R}}$$

in general, the reduced formula can be applied as long as the dynamic range of the incident radiation is greater than 20 dB and the dark current in the device is less than 100 nA/cm².

Note that this analysis assumes that all random noise sources have been averaged to zero. The remaining noise sources that average to a DC level are included in the dark current term. The resulting contrast degradation is superimposed onto the MTF response of the device (i.e., it scales down the MTF curve).

Example: Under the following conditions (either equation applies) the contrast becomes:

E_{\max}	=	$5 \cdot 10^{14}$ photons/sec-cm ²	η	=	25%
E_{\min}	=	$1 \cdot 10^{12}$ photons/sec-cm ²	A_d	=	$(15 \mu\text{m})^2$
n	=	$J_d A_d / q = 1.4 \cdot 10^4$ electrons/sec (for a dark current of 1 nA/cm^2)			
		$\alpha = 1$ and $R = 17$	\Rightarrow		$C = 89\%$
		$\alpha = 1$ and $R = 3$	\Rightarrow		$C = 60\%$
		$\alpha = 1/2$ and $R = 17$	\Rightarrow		$C = 94\%$
		$\alpha = 1/2$ and $R = 3$	\Rightarrow		$C = 75\%$



APPENDIX E

SPICE SIMULATIONS

Polysilicon



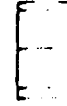
Oxide



Depletion Layer



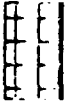
Epitaxial Layer



Substrate



A01



A02



A03



$t(\text{poly}) = 5000 \text{ \AA}$

$t(\text{oxide}) = 1000 \text{ \AA}$

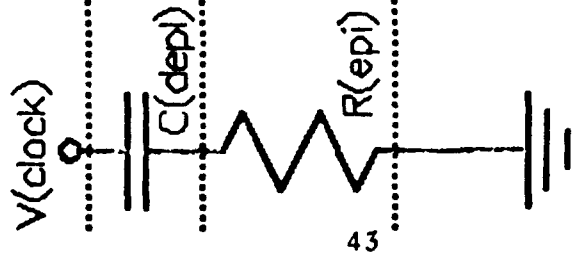
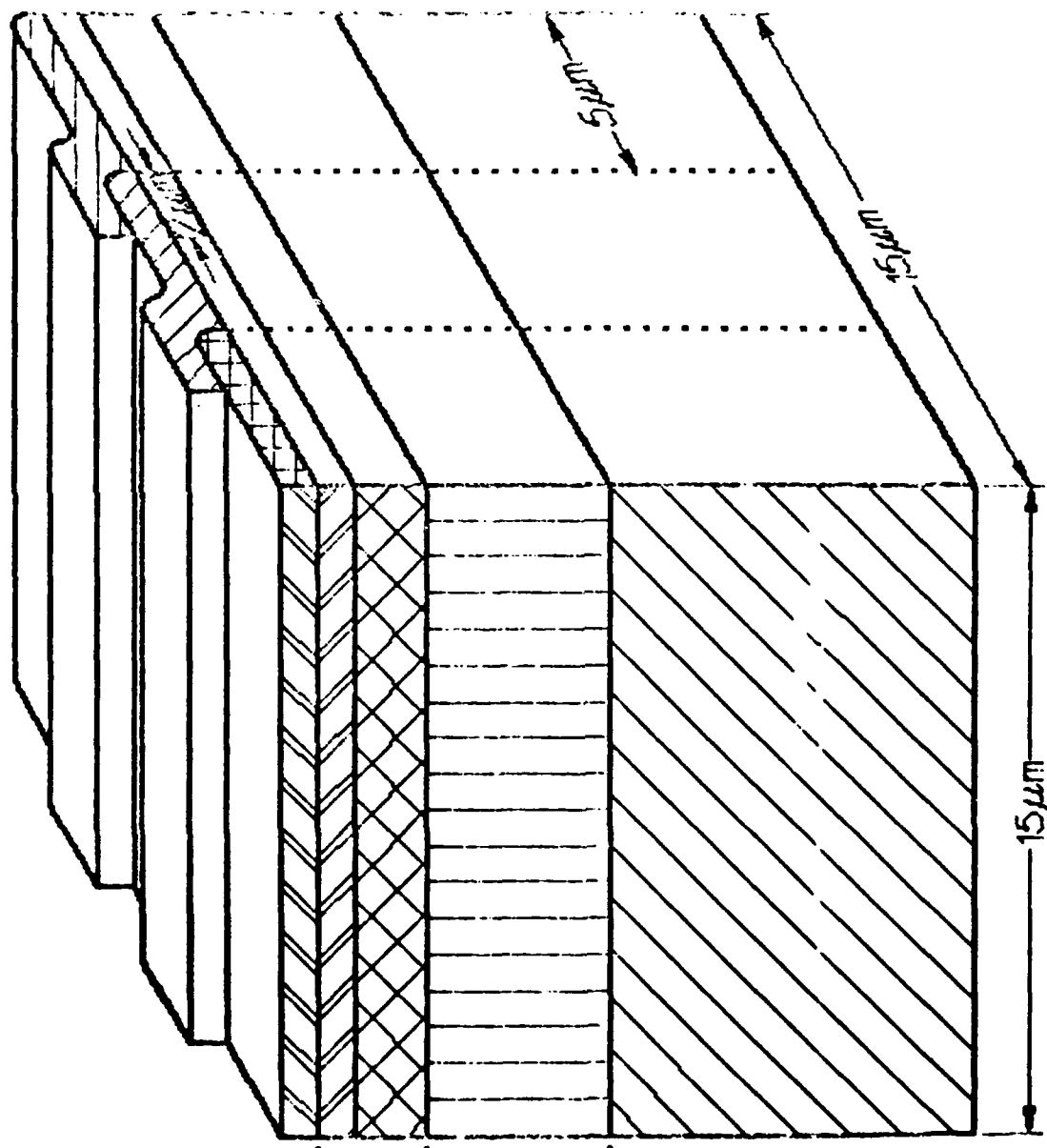
$t(\text{depl}) = 5 \text{ \mu m}$

$t(\text{epi}) = 15 \text{ \mu m}$

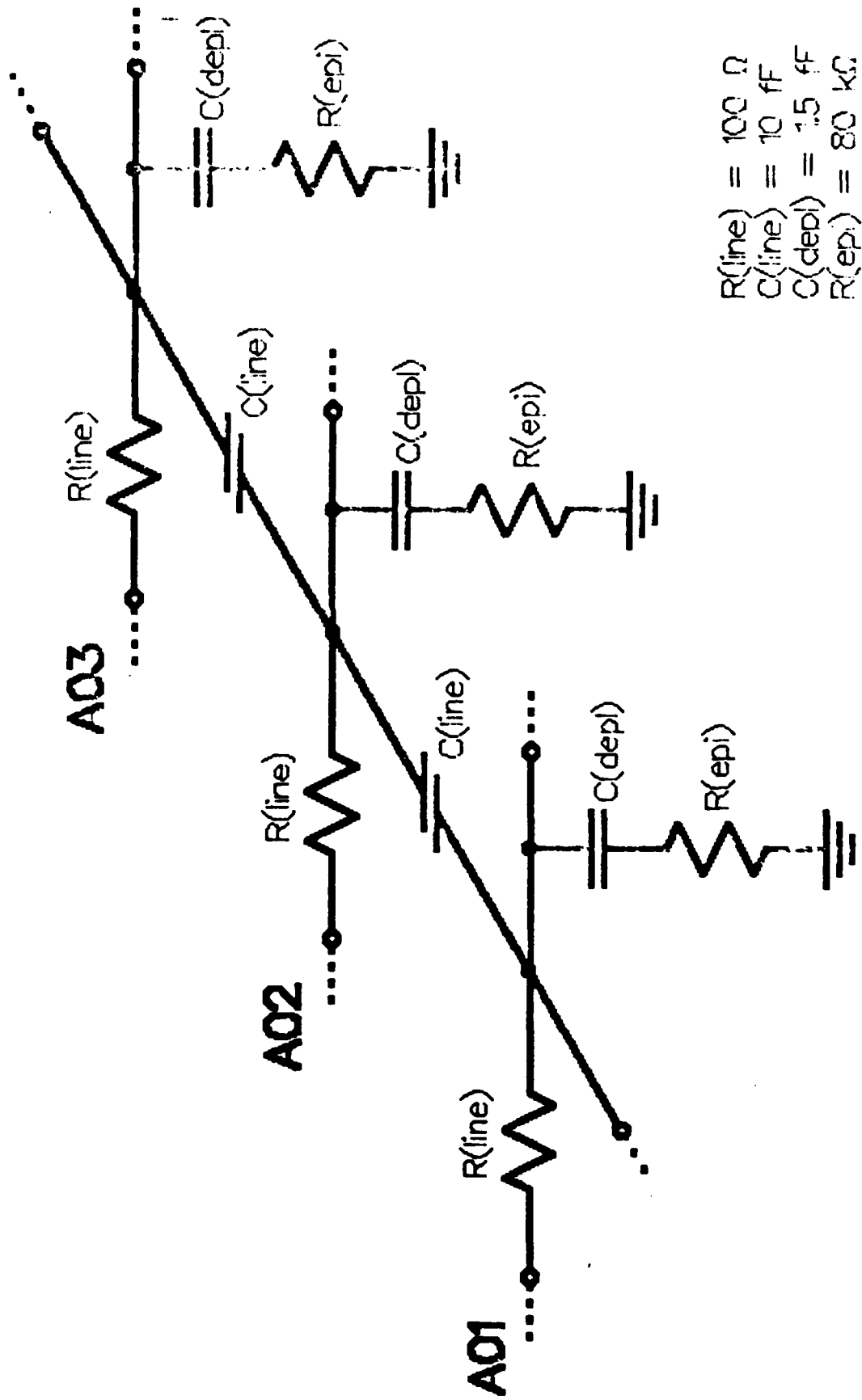
$t(\text{sub}) = 500 \text{ \mu m}$

$\rho(\text{epi}) = 40 \text{ \Omega-cm}$

$\rho(\text{sub}) = 0.01 \text{ \Omega-cm}$



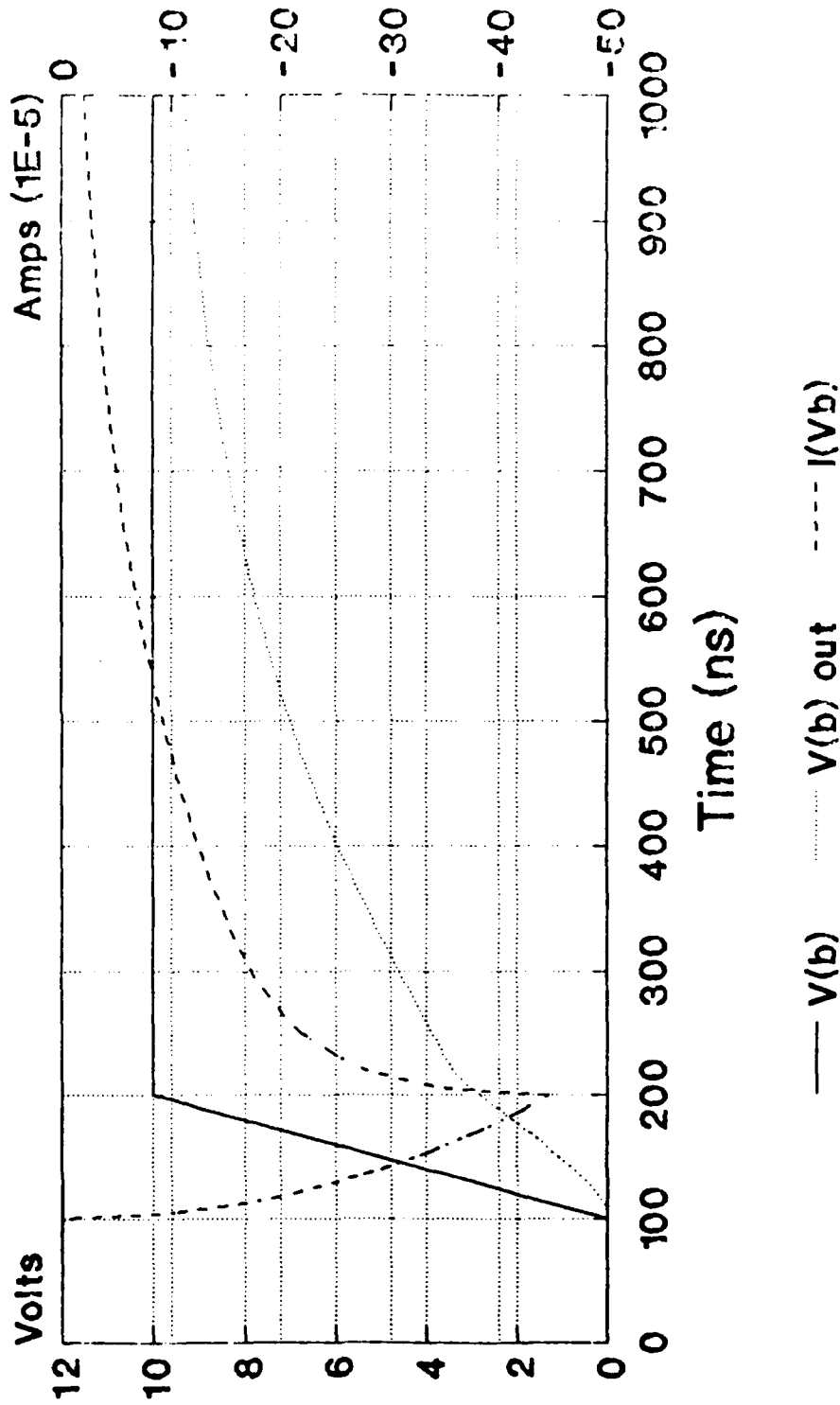
Ford F1024B Focal Plane Array Model



Ford F1024B Array Clock Model

F1024B Clock Line Simulation

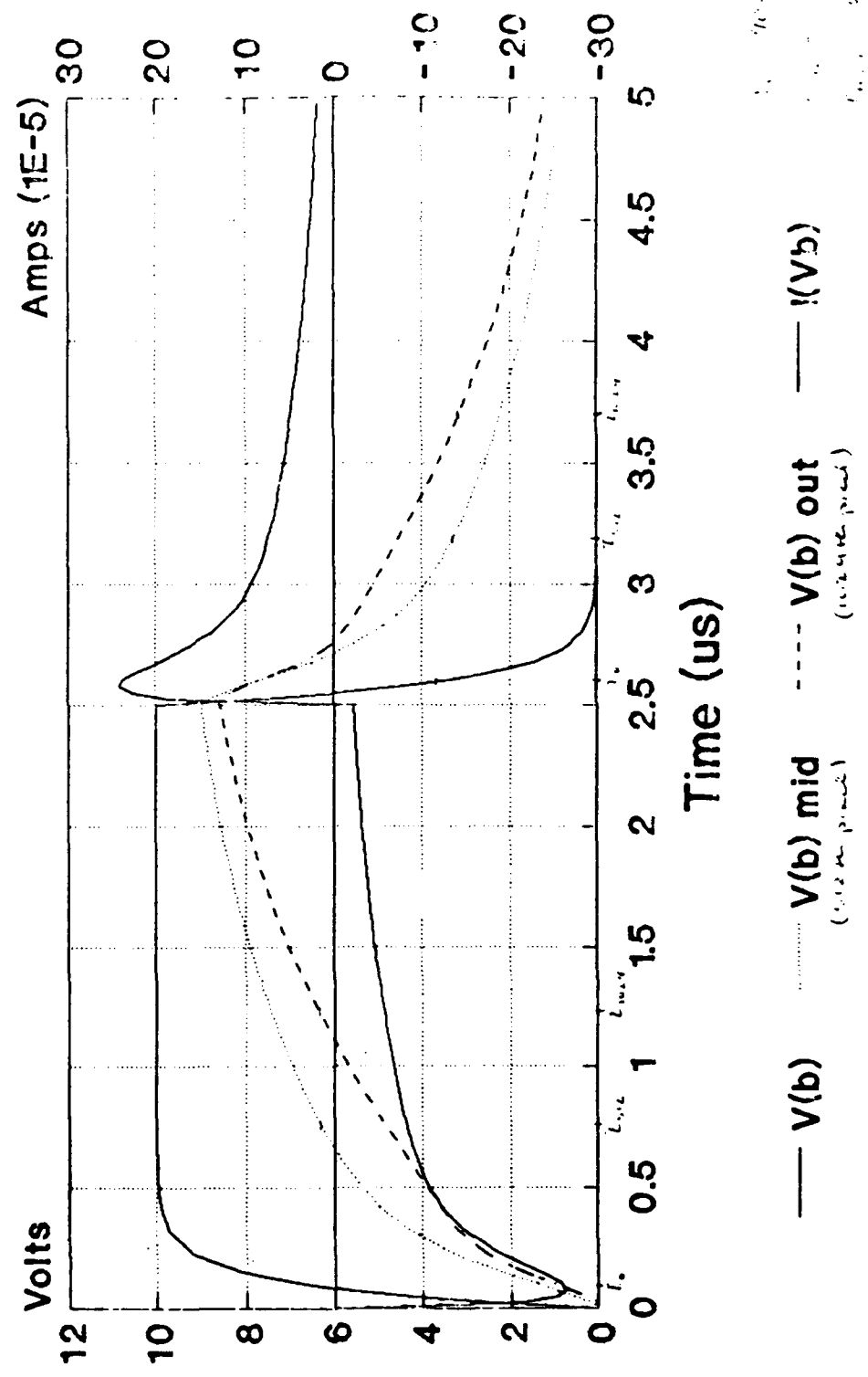
Triple Line -- Single Rising Edge



(Spice Analysis from 1/30/91)

F1024B Clock Line Simulation

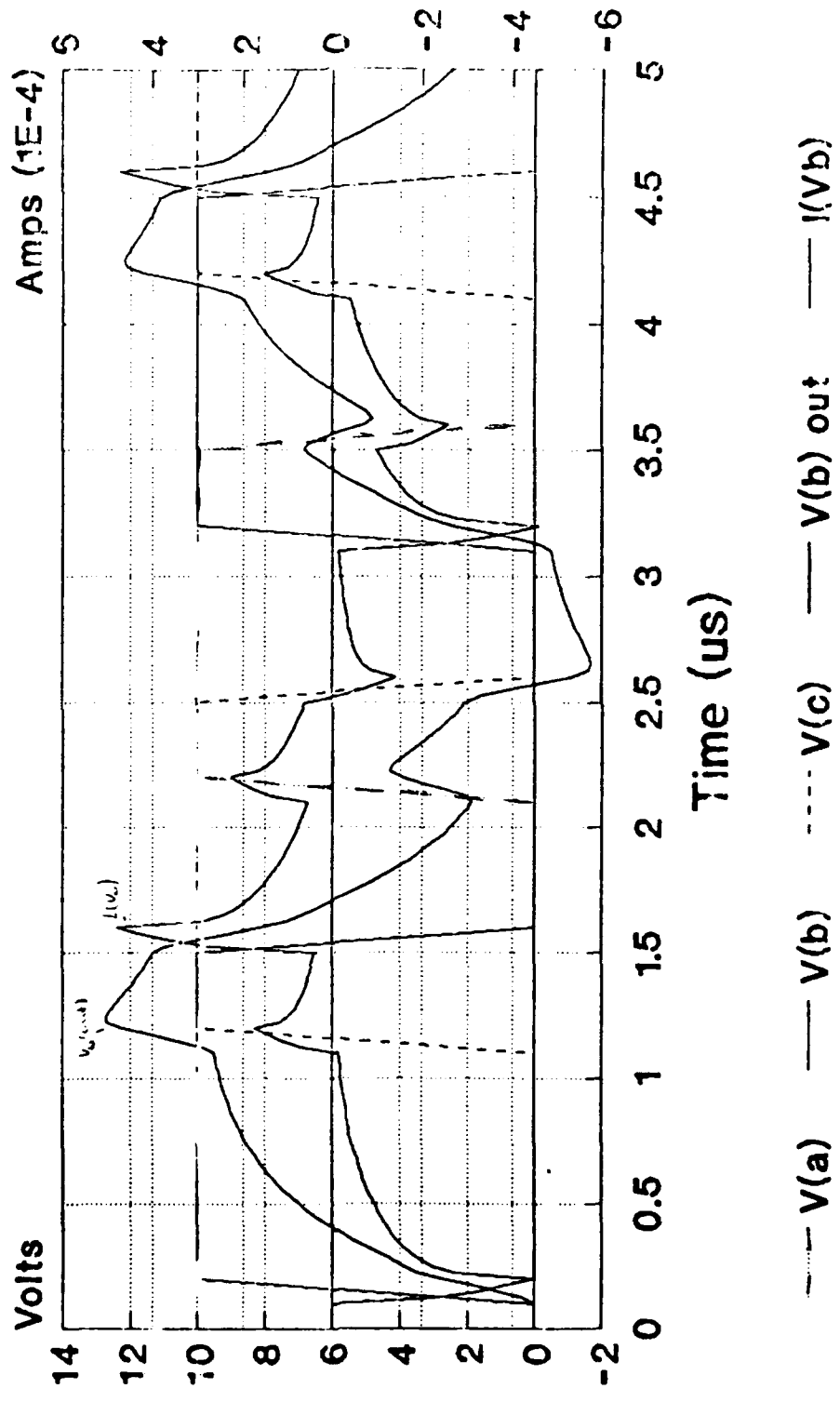
Triple 1024-pixel Clock Line



(Spice Analysis from 2/7/91)

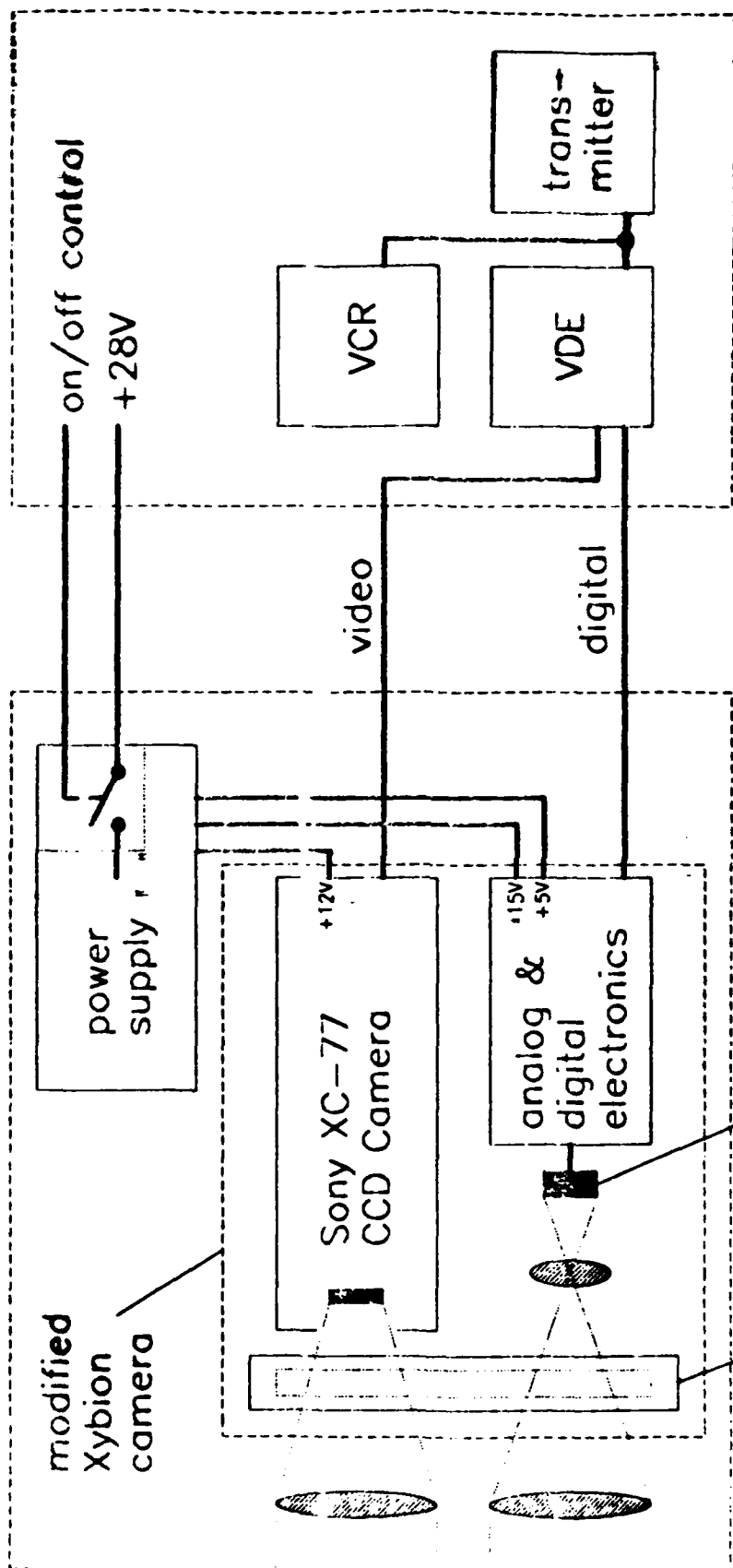
F1024B Clock Line Simulation

Triple Line -- 333kHz Clock

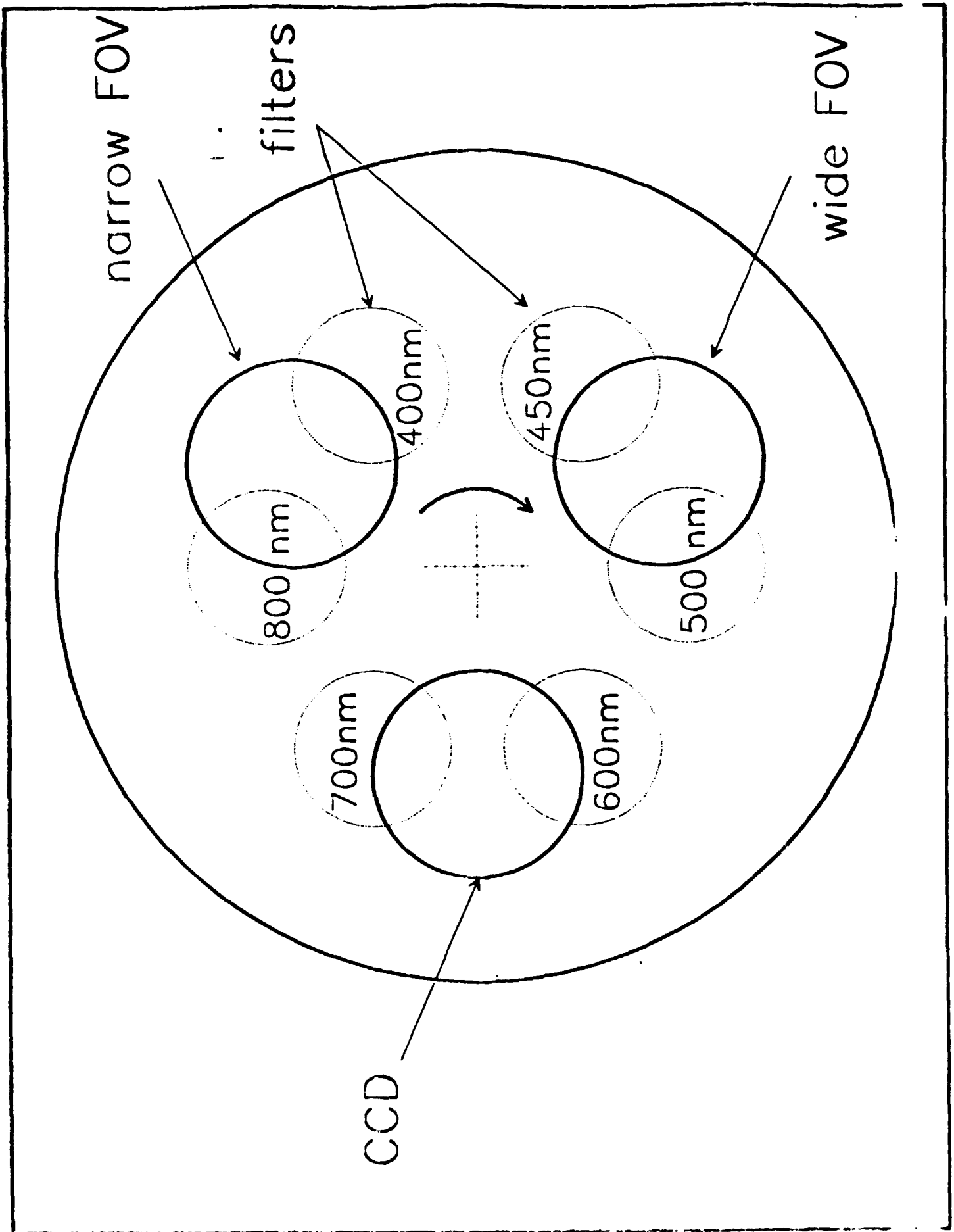


(Spice Analysis from 2/6/91)

APPENDIX F
MULTISPECTRAL RADIOMETER



filter wheel photodiode



Multispectral Radiometer: System Specifications

dimensions:	24" (L) x 8" (W) x 12" (H)																		
weight:	80 lbs.																		
power requirements;	28 Vdc, 2 amps																		
operating temp.:	-15 °C to 40 °C																		
video output:	EIA standard, see Xybion camera specs																		
data output:	8-bit parallel interface to Datum Video Data Encoder																		
camera:	30.8° (H) x 23.3° (V) field of view 16mm, F/1.4 lens																		
WFOV radiometer:	24.2° circular field of view 50 mm, F/1.8 lens dynamic range from 1 nW/cm ² -sr to 0.85 mW/cm ² -sr extended source radiance at maximum iris, depending on filter average standard deviation on 50 samples is 9.6 D.N.																		
NFOV radiometer:	4° circular field of view 135 mm, F/2.8 lens dynamic range from 50 nW/cm ² -sr to 2 mW/cm ² -sr extended source radiance at maximum iris, depending on filter average standard deviation on 50 samples is 11.5 D.N.																		
data capture rate:	60 samples/sec																		
spectral filters:	<table><thead><tr><th>filter #</th><th>wavelength</th><th>bandwidth</th></tr></thead><tbody><tr><td>1</td><td>400 nm</td><td>70 nm</td></tr><tr><td>2</td><td>450 nm</td><td>80 nm</td></tr><tr><td>3</td><td>500 nm</td><td>80 nm</td></tr><tr><td>4</td><td>600 nm</td><td>80 nm</td></tr><tr><td>5</td><td>700 nm</td><td>80 nm</td></tr></tbody></table>	filter #	wavelength	bandwidth	1	400 nm	70 nm	2	450 nm	80 nm	3	500 nm	80 nm	4	600 nm	80 nm	5	700 nm	80 nm
filter #	wavelength	bandwidth																	
1	400 nm	70 nm																	
2	450 nm	80 nm																	
3	500 nm	80 nm																	
4	600 nm	80 nm																	
5	700 nm	80 nm																	